Available online at www.sciencedirect.com
SCIENCE DIRECT®
International Journal of Multiphase Flow 30 (2004) 995–1010
International Journal of Multiphase Flow
www.elsevier.com/locate/ijmulflow

Multiphase water flow inside carbon nanotubes ☆

E.M. Kotsalis, J.H. Walther, P. Koumoutsakos *

Institute of Computational Science, ETH Zurich, Hirschengrabenstrasse 84, 8092 Zurich, Switzerland

Received 22 December 2003; received in revised form 15 March 2004

Abstract

We present nonequilibrium molecular dynamics simulations of the flow of liquid–vapour water mixtures and mixtures of water and nitrogen inside carbon nanotubes. A new adaptive forcing scheme is proposed to impose a mean flow through the system. The flow of liquid water is characterised by a distinct layering of the water molecules in the vicinity of the boundary and a slip length that is found to increase with the radius of the carbon nanotube. Increasing the temperature and pressure of the system furthermore results in a decrease in the slip length. For the flow of mixtures of nitrogen and water we find that the slip length is reduced as compared to the slip for the pure water. The shorter slip length is attributed to the fact that nitrogen forms droplets at the carbon surface, thus partially shielding the bulk flow from the hydrophobic carbon surface.

Keywords: Multiphase flow; Carbon nanotubes; Slip length; Water–nitrogen mixture; Confined fluid

1. Introduction

An understanding of the interaction of water with carbon in confined geometries at the nanoscale is very important for exploring the potential of devices such as carbon nanotubes (CNT) in nanofluidic chips and capsules for drug delivery. The nanotube cavities are weakly reacting with a large number of substances and may serve as nanosize test tubes. The prospect of

☆ This paper is dedicated to Professor George Yadigaroglou for the occasion of his 65th birthday. George has been a mentor by example for the last author and he has been an inspiration on how to combine quality, imagination and rigor in life and in research. He is one of the leading researchers in the area of multiphase fluid mechanics and we hope to continue his spirit in our research in multiphase flow phenomena in the nanoscale.

* Corresponding author.
E-mail addresses: kotsalie@inf.ethz.ch (E.M. Kotsalis), walther@inf.ethz.ch (J.H. Walther), petros@inf.ethz.ch (P. Koumoutsakos).

0301-9322/$ - see front matter
doi:10.1016/j.ijmultiphaseflow.2004.03.009

controlled transport of picoliter volumes of fluid and single molecules requires addressing phenomena such as local density increase of several orders of magnitude and layering of transported elements in confined nanoscale geometries (Israelachvili et al., 1988). In addition the ability to encapsulate a material in a nanotube also offers new possibilities for investigating dimensionally confined phase transitions. In particular, water molecules in confinement exhibit several phase transitions as their network of hydrogen bonds is disrupted.

Experiments have demonstrated that fluid properties become drastically altered when the separation between solid surfaces approaches the atomic scale (Chan and Horn, 1985; Gee et al., 1990). In the case of water, so-called drying transitions occure on this scale as a result of strong hydrogen-bonding between water molecules, which can cause the liquid to recede from nonpolar surfaces and form distinct layers separating the bulk phase from the surface (Granick, 1991).

Computational studies have played an important role in understanding the behaviour of fluids in the nanometer scale, complementing experimental works. A detailed study regarding the behaviour of a fluid in confinement was reported in Thompson and Robbins (1990) with molecular dynamics simulations of Lennard–Jones liquids sheared between two solid walls. Confinement of water in nanoscales (Koga et al., 2002) can induce properties that correspond to water properties in supercritical conditions. At room temperature, water is forming tetrahedral units of five molecules linked by hydrogen bonds but when the temperature is raised and/or density is reduced, some of the hydrogen bonds are broken. Most of the dominant order is then lost and the remaining structures are linear and bifurcated chains of hydrogen bonded water molecules which can be regarded as parts of broken tetrahedrals. The destruction of the hydrogen bonds affects the water such so that its compressibility and transport properties are intermediate between those of liquid and gas.

Meso and macroscopic modeling of problems in nanoscale fluid mechanics may prove a computationally cost effective alternative to molecular dynamics simulations (Koplik and Banavar, 1995) usually employed at these length scales. However as the surface to volume ratio in these flows is large the development of appropriate boundary conditions is of paramount importance and it is necessary that the complex fluid–solid interactions can be described by a suitable macroscopic model. At hydrophobic interfaces these interactions typically result in a finite fluid slip velocity (ΔU) (Helmholtz and von Piotrowski, 1860; Schnell, 1956; Churaev et al., 1984; Baudry et al., 2001). At moderate shear rates ($\partial u/\partial y$) the slip velocity may be described by the linear relation (Loose and Hess, 1989):

$$\Delta U = L_s \frac{\partial u}{\partial y}, \tag{1}$$

where L_s is the slip length. Experimental evidence of slip has been demonstrated in studies of water in hydrophobized quartz capillaries (Churaev et al., 1984) and in drainage experiments (Baudry et al., 2001) with slip lengths of 30 ± 10 and 38 ± 2 nm, respectively. While most experiments have focused on the presence of slip at hydrophobic surfaces and on the possible validity of the no-slip condition at hydrophilic surfaces, recent colloid probe experiments of water on mica and glass have indicated a persistent slip of 8–9 nm at these hydrophilic surfaces (Bonaccurso et al., 2002). Molecular dynamics simulations of Poiseuille flow (Barrat and Bocquet, 1999; Travis et al., 1997;

Travis and Gubbins, 2000) and planar Couette flow (Thompson and Robbins, 1990; Thompson and Troian, 1997; Cieplak et al., 2001) of simple Lennard–Jones fluids confined between Lennard–Jones solids have demonstrated the presence of both slip, no-slip and locking (negative slip length) depending on the corrugation of the surface. Slip of simple fluids such as methane inside CNT's was recently studied by Sokhan et al. (2002). They found that the flow is characterised by a significant slip of 6.9–7.3 nm for $(10, 10)$ to $(20, 20)$ tubes and an approximately 1 nm smaller slip if the tubes were treated as rigid structures.

In the present paper, we study the flow of water inside CNTs of different diameters at a variety of temperatures and pressures. The amount of slip expected at the surface is largely determined by the ability of water to wet carbon nanotubes. While early experiments (Dujardin et al., 1998) indicated that liquids such as water with a surface tension below 130–170 mN/m would wet bundles of single-wall carbon nanotubes, and wetting was observed in multiwall CNT by aqueous inclusions composed of 85.2% water, 7.4% CO_2 and 7.4% CH_4 (Gogotsi et al., 2001), molecular dynamics simulations (Werder et al., 2001) predicted that pristine carbon nanotubes would be hydrophobic. The latter finding is in agreement with the low solubility of CNTs in water (Bahr et al., 2001). The paper is organised as follows: in Section 2 we outline the physical problem and describe the nonequilibrium molecular dynamics (NEMD) employed in the present study. In Section 3 we discuss the results of the simulations and the paper concludes with a summary of the results presented herein.

2. Multiphase flow in carbon nanotubes

We consider steady-state Poiseuille-like flow through a single-wall CNT of liquid and vapour water mixtures and flow of a water–nitrogen mixture. A constant flow rate is achieved through the use of a new adaptive forcing scheme that imposes a mean center-of-mass velocity. This scheme is found to compare favorably with the nonadaptive gravity-like force scheme (Sokhan et al., 2001). A mean flow speed of 100 m s^{-1} is used throughout to secure low Mach numbers, while sufficiently above the thermal noise to allow efficient sampling.

2.1. Nonequilibrium molecular dynamics

The present study employs nonequilibrium molecular dynamics (NEMD) simulations of isothermal Poiseuille flow. The fluid molecules are initially placed on a regular lattice and the tube is filled using a trial-and-error procedure until the desired pressure level is achieved. The pressure is measured as the radial component of the forces acting on carbon atoms of the nanotube per unit area. During the initial equilibration the flow is at rest and the system is coupled to a Berendsen thermostat (Berendsen et al., 1984) to achieve the desired temperature. After the equilibration, the fluid is set into motion, and in order to avoid viscous heating, the system is then coupled to a two-dimensional thermostat. Thus, the temperature is given by

$$T = \frac{2}{n_{\mathrm{dof}} N k_{\mathrm{B}}} \sum_{i=1}^{n_{\mathrm{dof}}} E^i_{\mathrm{kin}}, \tag{2}$$

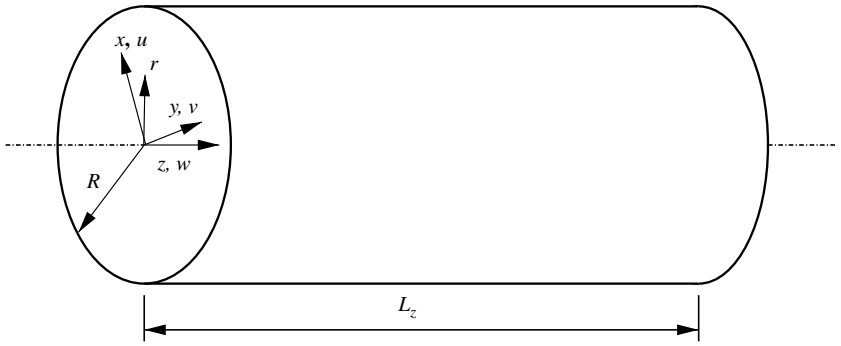

Fig. 1. Schematic of the system. R and z denote the radius of and the axis of the carbon nanotube. The size of the computational box along z is L_z.

where n_{dof} is the number of degrees of freedom (here $n_{\mathrm{dof}} = 2$), N the number of water molecules, k_{B} the Boltzmann constant and E^1_{kin}, E^2_{kin} are the kinetic energies of the water molecules in the x and y-direction (cf. Fig. 1). The Berendsen thermostat involves a scaling of the velocities, thus

$$\tilde{v}_x = \lambda v_x, \qquad \tilde{v}_y = \lambda v_y, \tag{3}$$

where

$$\lambda = \left[1 - \frac{\delta t}{\tau}\left(\frac{T_{\mathrm{tar}}}{T} - 1\right)\right]^{1/2}, \tag{4}$$

and δt is the time step, T_{tar} the target temperature, and τ is the time constant of the thermostat. The carbon nanotube is modeled atomistically, but treated as a rigid structure to allow the maximum time step of 2 fs imposed by the water model and to simplify the sampling. The influence of modeling the carbon nanotube as a rigid structure was recently found to be negligible for the static properties of water at carbon surfaces (Werder et al., 2001, 2003) and to be of secondary importance for dynamic properties such as the amount of slip (Sokhan et al., 2002).

2.1.1. Interaction potentials

The water is modeled using the rigid SPC/E water model by Berendsen et al. (1987), with an O–H bond length of 1 Å and a H–O–H angle of 109.47° constrained using the SHAKE algorithm (van Gunsteren and Berendsen, 1977). The SPC/E model involves a Lennard–Jones potential between the oxygen atoms

$$U_{\alpha\beta}(r_{ij}) = 4\epsilon_{\alpha\beta}\left[\left(\frac{\sigma_{\alpha\beta}}{r_{ij}}\right)^{12} - \left(\frac{\sigma_{\alpha\beta}}{r_{ij}}\right)^{6}\right] \quad \text{for } r_{ij} < r_{\mathrm{c}}, \tag{5}$$

where r_{c} is the radius of truncation ($U_{\alpha\beta}(r_{ij}) = 0$ for $r_{ij} > r_{\mathrm{c}}$), and α and β refers to the atomic species (here oxygen–oxygen: $\epsilon_{\mathrm{OO}} = 0.6501\ \mathrm{kJ\,mol^{-1}}$ and $\sigma_{\mathrm{OO}} = 0.3166$ nm). The model furthermore involves a Coulomb potential acting between all atom pairs from different water molecules

$$U(r_{ij}) = \frac{q_i q_j}{4\pi\epsilon_0}\frac{1}{r_{ij}}, \tag{6}$$

where ϵ_0 is the permittivity in vacuum, and q_i is the partial charge, $q_O = -0.8476$ and $q_H = 0.4238$, respectively. These partial charges describe the fixed, static dipole moment of the water molecule (Berendsen et al., 1987). The present study uses a smooth truncation at 1.0 nm of the Coulomb interaction as described in Walther et al. (2001).

For simplicity, the nitrogen (N_2) molecules are treated as single Lennard–Jones sites with the parameters obtained from Bojan and Steele (1987), thus $\epsilon_{N_2N_2} = 0.2776$ kJ mol^{-1} and $\sigma_{N_2N_2} = 0.3360$ nm, respectively. Given these interaction potentials for the fluids, the wetting properties of the fluid–solid interface, and the ability of the interface to resist shear leading to a slip or no-slip condition, is determined by the potential function governing the fluid–solid interaction. For the water–carbon interaction we use a Lennard–Jones potential between the carbon and oxygen atoms of the water, with values from Werder et al. (2003) of $\epsilon_{CO} = 0.392$ kJ mol^{-1} and $\sigma_{CO} = 0.3190$ nm. These values reproduce the experimental contact angle of water droplets in contact with a graphite surface (Werder et al., 2003; Fowkes and Harkins, 1940).

The Lennard–Jones parameters for N_2 are obtained by applying the Berthelot–Lorentz mixing rules

$$\epsilon_{N_2\beta} = \sqrt{\epsilon_{N_2N_2}\epsilon_{\beta\beta}}, \quad \sigma_{N_2\beta} = \tfrac{1}{2}(\sigma_{N_2N_2} + \sigma_{\beta\beta}), \qquad \beta = O, C \tag{7}$$

thus the N_2 parameters are $\epsilon_{N_2C} = 0.2540$ kJ mol^{-1}, $\sigma_{N_2C} = 0.3380$ nm, $\epsilon_{N_2O} = 0.4248$ kJ mol^{-1}, and $\sigma_{N_2O} = 0.3263$ nm.

The governing Newton's equations are integrated in time using the leapfrog scheme subject to quasi-periodic boundary conditions in the direction along the axis of the carbon nanotube (z-axis) as shown in Fig. 1.

2.1.2. Time integration and forcing

The forcing of a mean flow in molecular dynamics simulations is usually achieved by imposing an acceleration (''gravity'') on each fluid atom in the system. Typical values for the acceleration is 10^{11}–10^{12} m s^{-2} (Sokhan et al., 2001) depending on the amount friction exerted by the solid walls and the desired mean velocity. Thus, for the flow of methane in a carbon nanotube Sokhan et al. (2002) used an acceleration of 0.5×10^{12} m s^{-2} to attain a mean velocity of 57 m s^{-1}. However, this procedure may result in low frequency oscillations of the mean flow as observed by Sokhan et al. (2001) for two-dimensional Poiseuille flow of methane between graphite surfaces. These oscillations with wave lengths of 10 ps, 0.2 ns, and 2.0 ns extend the requirement for simulation time in order to sufficiently sample these slow modes. To improve the sampling rate, we propose an alternative adaptive scheme in which the imposed acceleration is computed dynamically to secure the desired (fixed) mean flow. Thus in a leapfrog approximation, the velocity of the molecules is updated according to

$$\boldsymbol{v}_i^{n+1/2} = \boldsymbol{v}_i^{n-1/2} + \frac{\delta t}{m_i^n}\left(\boldsymbol{f}_i^n + \boldsymbol{b}^n\right), \tag{8}$$

where δt is the time step, $\boldsymbol{v}_i$ and m_i^n the velocity and mass of the ith molecule, and $\boldsymbol{f}_i^n$ and $\boldsymbol{b}^n$ denote the force and body force on the molecule, respectively. The center-of-mass velocity of the fluid molecules is updated accordingly

$$\boldsymbol{v}_{\mathrm{com}}^{n+1/2} = \boldsymbol{v}_{\mathrm{com}}^{n-1/2} + \frac{\delta t}{m_{\mathrm{tot}}^{n}} \left(\boldsymbol{f}_{\mathrm{tot}}^{n} + \boldsymbol{b}_{\mathrm{tot}}^{n} \right), \tag{9}$$

where $\boldsymbol{f}_{\mathrm{tot}}^{n}$ is the total force acting on the center of mass of the molecules, and $\boldsymbol{b}_{\mathrm{tot}}^{n}$ is the total body force. In Eq. (9), $\boldsymbol{b}_{\mathrm{tot}}^{n}$ is adjusted to yield the desired center-of-mass velocity ($\boldsymbol{v}_{\mathrm{com}}^{n+1/2} = \boldsymbol{U}$), thus

$$\boldsymbol{b}_{\mathrm{tot}}^{n} = \frac{m_{\mathrm{tot}}^{n}}{\delta t} \left(\boldsymbol{U} - \boldsymbol{v}_{\mathrm{com}}^{n-1/2} \right) - \boldsymbol{f}_{\mathrm{tot}}^{n}. \tag{10}$$

We have performed an extensive validation of the present scheme Kassinos et al. (in press) and compared the results from simulations of methane flowing in a carbon nanotube using a constant and the adaptive acceleration scheme.

3. Results

The simulations of fluids under confinement require a trial-and-error procedure in order to identify the number of molecules of the liquid to achieve the desired system pressure or equivalently the chemical potential (Sokhan et al., 2002). This procedure is complicated by the large fluctuations in the pressure and the sensitivity of the pressure to the number of molecules. As an example, by removing five water molecules from the system considered (cf. Table 1) the pressure decreases 160 bar. During the equilibration, the pressure is measured as the radial component of the force acting on the carbon atoms per unit area, and the number of molecules is adjusted to obtain the desired pressure.

The ability of the fluid–solid interface to resist shear and the resulting macroscopic boundary condition is measured from the time average streaming velocity

$$\boldsymbol{u}_k = \frac{\sum_i^{n_k} m_i \boldsymbol{v}_i}{\sum_i^{n_k} m_i}, \tag{11}$$

where m_i and $\boldsymbol{v}_i$ are the mass and velocity of the ith atom, and n_k denotes the number of atoms in the kth bin. The statistics are sampled in polar bins of constant volume. The slip length (L_{s}) is extracted from the time average velocity profiles (11) using a least square fit to the parabola

$$w(r) = Ar^2 + Br + C. \tag{12}$$

Assuming $\partial w/\partial r|_{r=0} = 0$ gives $B = 0$ and thus a slip length of $L_{\mathrm{s}} = \sqrt{-C/A} - R$. The fitting is performed on the data in the interval $r \in [0 : R - \delta]$, where δ is adjusted to obtain a standard deviation of the slip length based on the number of bins considered less than 1 nm. We used values of δ of 0.22, 0.23, 0.24, and 0.25 nm. For all the simulations summarized in Table 1 the presented mean of the slip lengths is obtained from these four least square fits. For the calculation of the slip length all the simulations have been conducted up to 10 ns collecting statistics from 1 to 10 ns with a total of 45 000 snapshots. One simulation (case 8) was continued until 19 ns and the resulting slip length was found to be the same independent of the sampling interval (1–10 or 10–19 ns).

Table 1
Overview of the simulation cases

Cases	Ch	N_{H_2O}	N_{N_2}	T (K)	p (bar)	L (nm)
1	(20, 20)	736	0	300	811 ± 554	11
2	(20, 20)	736	0	500	4644 ± 887	7
3	(20, 20)	416	0	300	-419 ± 366	14
4	(20, 20)	416	0	500	-289 ± 431	8
5	(20, 20)	416	0	700	881 ± 643	5
6	(20, 20)	208	0	500	-133 ± 314	7
7	(20, 20)	208	0	1000	922 ± 615	5
8	(20, 20)	208	0	1500	1975 ± 903	4
9	(20, 20)	644	50	300	948 ± 542	9
10	(30, 30)	904	0	300	605 ± 640	13
11	(40, 40)	1694	0	300	706 ± 573	15

Ch denotes the chirality of the carbon nanotube, N_{H_2O} the number of water molecules, N_{N_2} the number of nitrogen molecules, L the slip length, and p the pressure with fluctuations given by the standard deviation of the instantaneous pressure.

3.1. Flow of liquid–vapour mixtures of water in carbon nanotubes

First we study the flow of water through carbon nanotubes of different diameters at a temperature of 300 K. The carbon nanotubes considered are armchair tubes with chirality vectors of (20, 20), (30, 30), and (40, 40), corresponding to tube diameters of 2.712, 4.068, and 5.424 nm, respectively. The mean flow speed is 100 m s^{-1} and the pressure in the system is in the range 600–800 bar sufficiently high to secure a complete filling of the tube. This pressure is achieved at a total number of water molecules of 736, 904, and 1694, respectively. Note that the pressure calculation exhibit large fluctuations ($\approx \pm 600$ bar) due to the small size of the system.

The slip lengths extracted from the streaming velocity profiles shown in Fig. 2 are 11, 13, and 15 nm, for the 2.712, 4.068, and 5.424 nm diameter tubes, respectively. The flow in the carbon

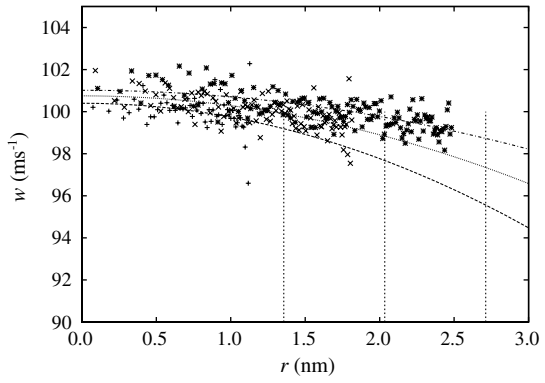

Fig. 2. Time average streaming velocity profiles of water in a carbon nanotubes of different diameter: 2.712 nm: (+, – –); 4.068 nm: (×, · · ·); 5.424 nm: (*, – · –). The points indicate the values extracted from the NEMD simulations and the lines a least squared fit to Eq. (12). The vertical lines mark the position of the surface of the carbon nanotubes.

nanotube with the smallest radius displays the smallest slip length, consistent with increasing surface friction due to curvature as the radius is reduced. The trends of the computed values indicate an agreement with the experimental value of 30 nm measured by Churaev et al. (1984) for water flowing over an extended hydrophobic surface.

A series of simulations (cases 1–9) have been conducted for the $(20, 20)$ carbon nanotube to investigate the effect of the liquid density and temperature on the characteristics of the flow. In case 1 we consider liquid flow inside a carbon nanotube at 300 K using 736 molecules. This serves as the reference case for the rest of the simulations. A remarkable feature of this flow is the layering of water molecules as it is indicated in the density profiles, $\rho(r)$, shown in Fig. 3. The profiles are presented separately for the oxygen and hydrogen atoms and nondimensionalized through $\rho^*(r) = \rho(r)/\rho(0)$. In this figure we observe a well correlated peak in the density of oxygen and hydrogen atoms at $r = 1.04$ nm in the vicinity of the wall of the carbon nanotube. The coinciding peaks of the two profiles indicate that the plane of the water molecules is tangential to the surface of the carbon nanotube. The result is consistent with prior equilibrium studies of water in external to a carbon nanotube (Walther et al., 2004) and implies an ubiquitous property of water–carbon nanotube interactions independent of the curvature of the wall. Further away from the wall this peak is followed by a low density area around 0.87 nm. Finally, a new layering of water with a relatively higher density exists at 0.75 nm. Note however that the peaks of oxygen and hydrogen atoms are not so well correlated as the water density achieves the bulk values as we approach the center of the carbon nanotube. This feature of the water flow inside the carbon nanotube is further demonstrated in snapshots of the flow at the time intervals of 1, 2, and 3 ns. In Fig. 4 we show a cross-section of the water molecules located in the region $r \in [0.95, R]$ nm, corresponding to the first layer close to the wall of the nanotube. One can observe a high density water layer as it is indicated by the cross-sectional view of the water inside the carbon nanotube.

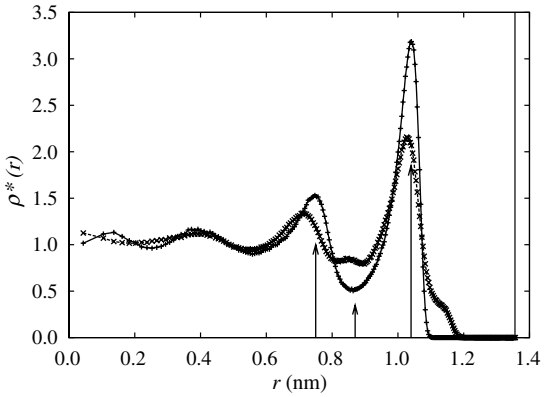

Fig. 3. Radial density profiles of oxygen (–+–) and hydrogen (–×–) atoms for case 1 averaged in the time interval [1–2] ns. The tube of a diameter of 2.712 nm is 100% filled with water molecules at a temperature of 300 K. The bulk density $\rho(0)$ is 1000 kg m^{-3}. The arrows denote the location of distinguishable layers of the water molecules and the vertical line the position of the CNT wall.

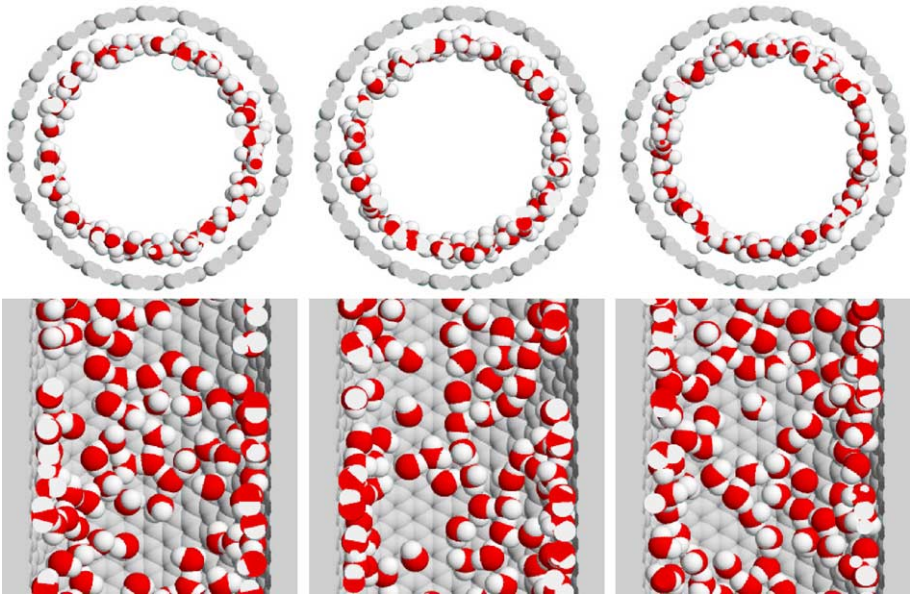

Fig. 4. Case 1: Snapshots of water molecules at 1, 2, and 3 ns (left to right) in the region $[0.95, R]$ nm indicating a high density layer near the wall of the carbon nanotube. Top figures correspond to cross-sections at the middle of the nanotube, while the bottom figures are showing radial cross-sections of this region.

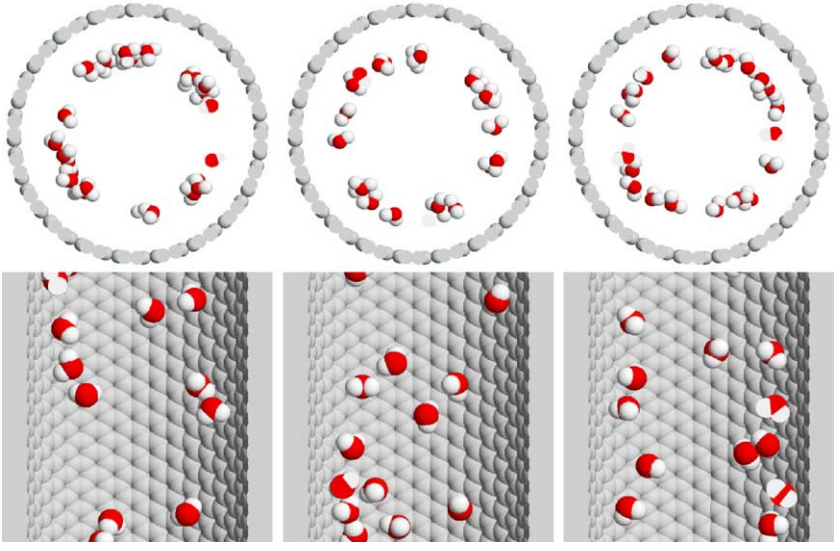

Fig. 5. Case 1: Snapshots of water molecules at 1, 2, and 3 ns (left to right) in the region $[0.79, 0.95]$ nm indicating a low density region away from the wall of the carbon nanotube. Top figures correspond to cross-sections at the middle of the nanotube, while the bottom figures are showing radial cross-sections of this region.

The axis parallel sections show an intricate network of water molecules, supported by a reduced number of hydrogen bonds that persists throughout the course of the simulations. Fig. 5 shows

the water molecules at the density minimum ($r \in [0.79–0.95]$ nm). This low density region is separating the high density layer of wall parallel water molecules from a layer with a less correlated configuration of oxygen and hydrogen atoms with relatively high density as shown in Fig. 6.

For the $(20, 20)$ carbon nanotube, an additional simulation was performed for the flow of liquid water at a temperature of 500 K corresponding to a pressure of 4644 bar (case 2). The velocity profile is compared with the results obtained at 300 K in Fig. 7a, and indicates a decrease in the slip length from 11 to 7 nm. The larger scatter observed at 500 K is attributed to the higher kinetic energy of the fluid. The radial density profiles for this flow are shown in Fig. 8a. A similar layering of the water molecules in three distinct regions is observed with a lesser correlated density of the oxygen and hydrogen atoms indicating a reduced wall parallel flow for the water molecules.

A series of simulations (cases 3–5) was performed in order to investigate the flow of liquid–vapour mixtures inside a $(20, 20)$ carbon nanotube. The carbon nanotube was partially filled (60%) with 416 water molecules and the simulations were performed at temperatures of 300, 500, and 700 K. For the case of 300 K the radial density profiles (Fig. 8b) indicate again a layering of the water molecules. However the flow behaviour is different as the flow corresponds to transport of alternating liquid and vapour clusters. With increasing temperature and pressure, the slip length decreases to 14, 8, and 5 nm respectively (cf. Table 1). The velocity profile of case 5 is compared to the reference case 1 in Fig. 7b.

At higher temperatures of 500 and 700 K the correlation of the radial density profile of the oxygen and the hydrogen atoms breaks down as it is indicated in Fig. 8c. These profiles and

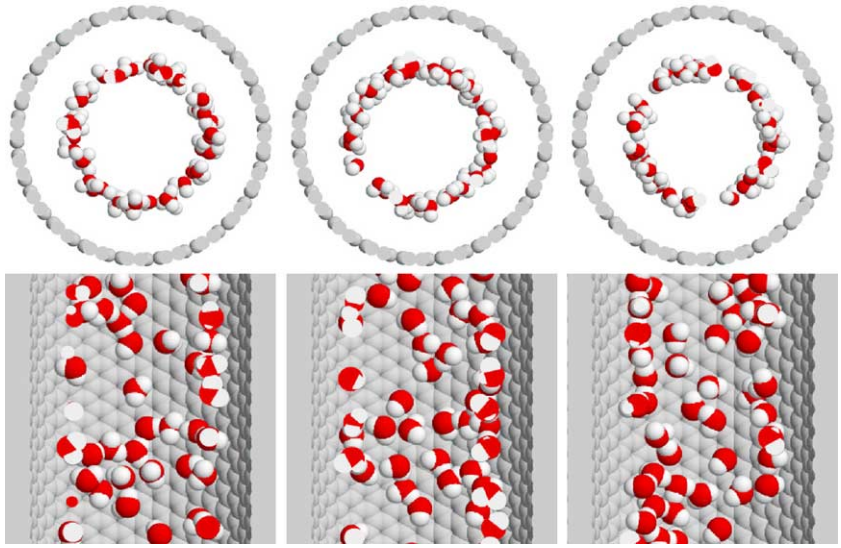

Fig. 6. Case 1: Snapshots of water molecules at 1, 2, and 3 ns (left to right) in the region $[0.63, 0.79]$ nm indicating a relatively high density liquid layer before the water exhibits bulk behaviour at the center of the carbon nanotube. Top figures correspond to cross-sections at the middle of the nanotube, while the bottom figures are showing radial cross-sections of this region.

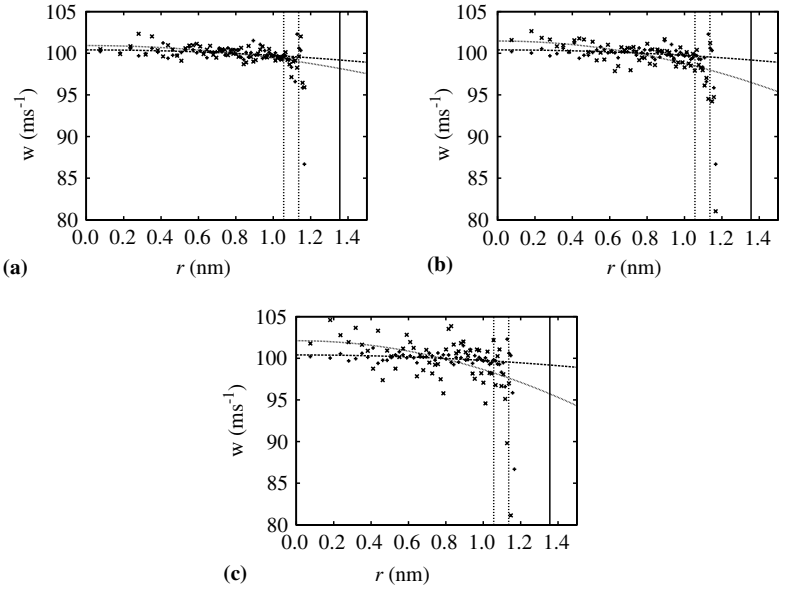

Fig. 7. Comparison of the velocity profiles for case 1 (liquid water at 300 K) (+, – –) and (a) case 2 (100% filled tube at 500 K), (b) case 5 (60% filled tube at 700 K) and (c) case 7 (30% filled tube at 1000 K) (×, ···) averaged over the time interval of [1–10] ns. The points indicate the values extracted from the NEMD simulations and the lines a least squared fit to Eq. (12) for $\delta = 0.22$ nm. The dashed vertical lines denote the minimum and maximum value of δ used for the fits. The thick vertical line marks the position of the CNT wall.

snapshots of the simulations (not shown here) indicate the consistent presence of a liquid water layer near the wall of the carbon nanotube while towards the center of the nanotube vapour bulk behaviour is observed. The distinct behaviour of the water layering in the case of liquid water versus liquid–vapour mixtures flowing inside the carbon nanotubes is shown in Fig. 9. In this figure one clearly observes the distinct layering in the case of liquid water inside the carbon nanotube (top) while the simulation of the liquid–vapour mixture only displays a weak structure.

By further decreasing the water density and for higher temperatures (500, 1000, and 1500 K) we achieve a flow of water vapour inside the carbon nanotubes (cases 6–8). The layered structure of the water molecules is strongly diminished and a rather uniform low vapour density is observed inside the carbon nanotube (Fig. 8d). For these cases, the increase in temperature and pressure again result in a reduction in the slip length to a value of 7, 5, and 4 nm respectively. The velocity profile of case 7 compared to the reference case 1 is shown in Fig. 7c.

3.2. Flow of water–nitrogen mixtures in carbon nanotubes

The effect of gas bubbles in hydrophobic systems is believed to influence the static properties of the system e.g., hydration (Attard et al., 2002), but also dynamic properties such as the amount of slip experienced at the fluid–solid interface (Vinogradova, 1999; Lauga and Stone, 2003). Thus,

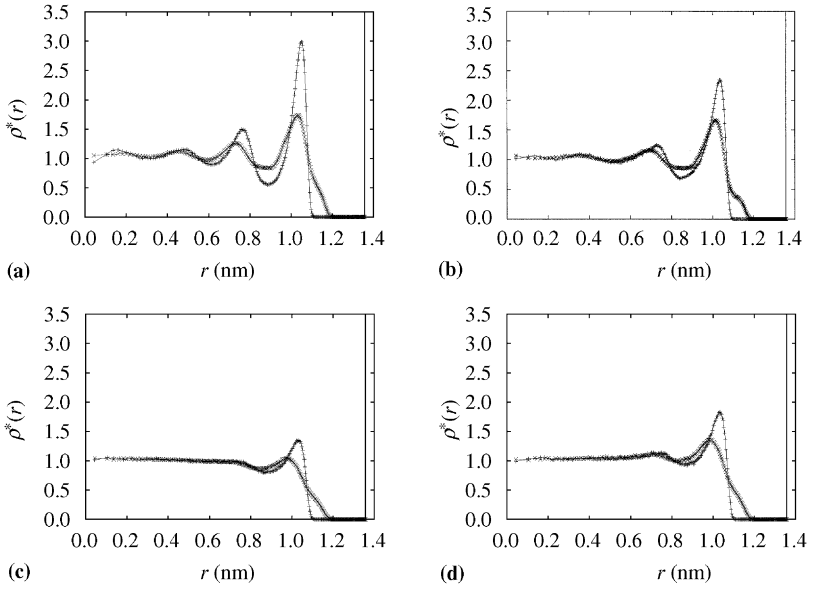

Fig. 8. Radial density profiles of oxygen and hydrogen atoms for cases 2, 3, 4, and 6 averaged in the time interval [1–2] ns. (a) The tube of diameter 2.712 nm, is 100% filled ($\rho(0) = 1000\ \mathrm{kg\,m^{-3}}$) with water molecules at a temperature of 500 K and the layering in three distinct layers is observed. The tube of diameter 2.712 nm, is 60% filled ($\rho(0) = 605$, 700 $\mathrm{kg\,m^{-3}}$, respectively) with water molecules at a temperature of (b) 300 and (c) 500 K, respectively. The distinct layering disappears by increasing the temperature. (d) The tube of diameter 2.712 nm is 30% filled ($\rho(0) = 305\ \mathrm{kg\,m^{-3}}$) with water molecules at a temperature of 500 K.

Lauga and Stone (2003) reported a series of experiments where the formation of nanobubbles on a hydrophobic surface would result in a zero-stress region leading to a relatively large slip length. However, the size of the bubbles reported in the experiments range from 35 to 600 nm exceeding the size of the present system by one or two orders of magnitude. Thus, to study these effects at the nanoscale, we consider a mixture of water and gas flowing inside a $(20, 20)$ carbon nanotube. The gas here is represented by nitrogen molecules dissolved in the water. At 300 K and 950 bar the employed molar concentration of N_2 of 0.078 M is supersaturated and corresponds to 50 nitrogen and 644 water molecules.

The forcing of the mean flow and the thermostat is only applied to the water molecules, which drives the system hydrodynamically and thermally. The nitrogen is initially placed randomly within the water as shown in Fig. 10a. During the equilibration of the system the nitrogen molecules desorp from the water phase forming high density, supercritical droplets at the carbon surface (see Fig. 10b).

The time average streaming velocity extracted from the trajectory in the time interval 1–10 ns is compared with the result from the pure water simulation (see Fig. 11). The extracted slip length is 9 nm approximately 2 nm less than slip experienced for pure water. The observed decrease in slip length is attributed to the fact that nitrogen forms supercritical droplets at the carbon surface, thus partially shielding the bulk flow from the hydrophobic carbon surface.

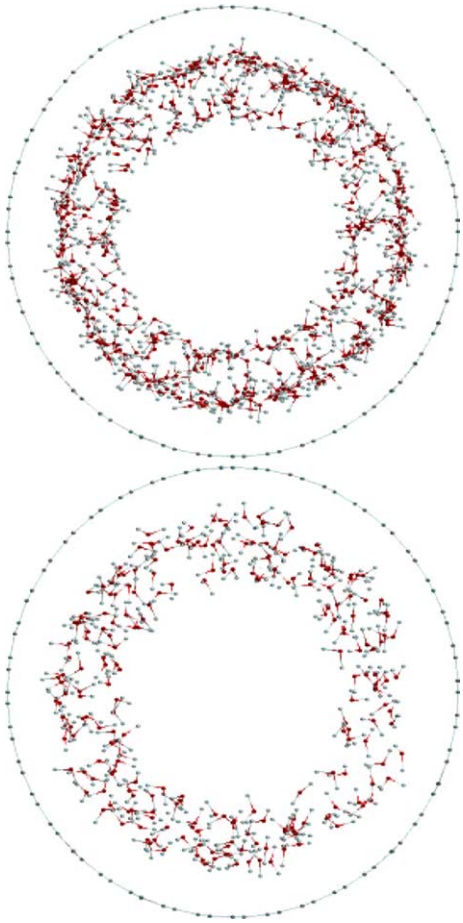

Fig. 9. Snapshots of the water molecules for the flow of liquid water flowing through a carbon nanotube at 300 K (top, case 1) and 500 K (bottom, case 4). The density variations and layering of the molecules observed at 300 K layers has virtually disappeared at 500 K.

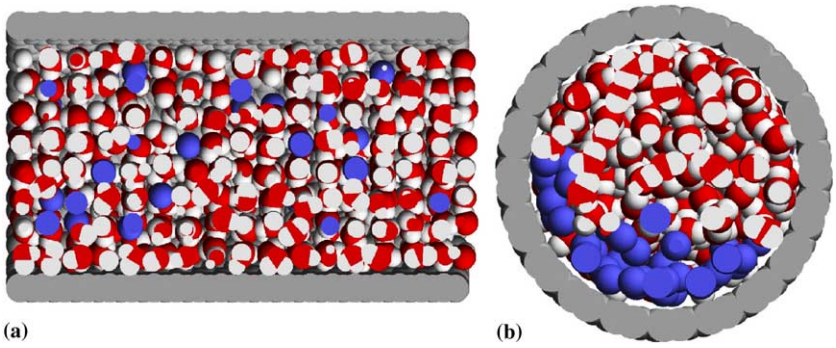

Fig. 10. Snapshots of the initial molecular configuration (a) and the equilibrated system (b) of a water–nitrogen mixture flowing inside a carbon nanotube.

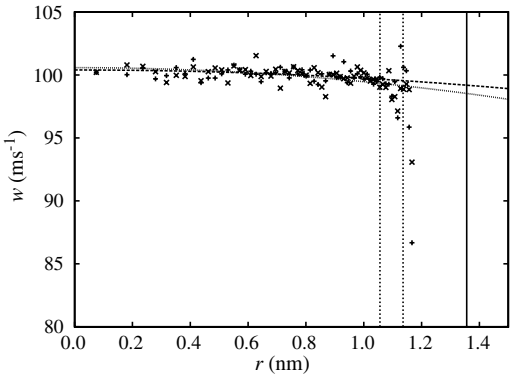

Fig. 11. Time average streaming velocity profiles of a water–nitrogen mixture (×, ···) in a carbon nanotube. The slip length is approximately 9 nm, and 2 nm, smaller than the corresponding results for pure water (+, ––). The points indicate the values extracted from the NEMD simulations and the lines a least squared fit to Eq. (12) for $\delta = 0.22$ nm. The dashed vertical lines denote the minimum and maximum value of δ used. The thick vertical line marks the position of the wall of the tube.

4. Summary

We have presented nonequilibrium molecular dynamics simulations of the multiphase flow of water and a water–nitrogen mixture inside carbon nanotubes. In these simulations we implemented a new adaptive scheme for imposing a mean fluid velocity through the system.

We found that flow in the confined geometries induces a layering of liquid water close to the walls of the carbon nanotube. The slip length of the flow is found to increase with increasing diameters of the carbon nanotube and followed by a decrease in the wall shear stress. For the case of a liquid–vapour mixture this layering is reduced and it is nonexistent for flow of vapour inside the nanotube. In the latter case the flow proceeds by transporting clusters of water molecules in liquid and vapour states without any particular layering near the nanotube walls.

We also considered the influence of nanobubbles on the slip length by performing simulations of mixtures of water and nitrogen. For this case we find a reduction of the slip length to 9 nm compared to the 11 nm of the pure system. We suspect that the shorter slip length in the case is due to the formation of supercritical nitrogen droplets at the carbon surface that partially shields the bulk flow from the hydrophobic carbon surface.

Acknowledgements

We wish to thank Thomas Werder, Urs Zimmerli and Pedro Gonnet for several helpful discussions throughout the work related to this manuscript.

References

Attard, P., Moody, M.P., Tyrrell, J.W.G., 2002. Nanobubbles: the big picture. Physica A 314, 696–705.

Bahr, J.L., Mickelson, E.T., Bronikowski, M.J., Smalley, R.E., Tour, J.M., 2001. Dissolution of small diameter single-wall carbon nanotubes in organic solvents? Chem. Commun. 2, 193–194.

Barrat, J.-L., Bocquet, L., 1999. Large slip effect at a nonwetting fluid–solid interface. Phys. Rev. Lett. 82, 4671–4674.
Baudry, J., Charlaix, E., Tonck, A., Mazuyer, D., 2001. Experimental evidence for a large slip effect at a nonwetting fluid–solid interface. Langmuir 17, 5232–5236.
Berendsen, H.J.C., Postma, J.P.M., van Gunsteren, W.F., DiNola, A., Haak, J.R., 1984. Molecular dynamics with coupling to an external bath. J. Chem. Phys. 81, 3684–3690.
Berendsen, H.J.C., Grigera, J.R., Straatsma, T.P., 1987. The missing term in effective pair potentials. J. Phys. Chem. 91, 6269–6271.
Bojan, M.J., Steele, W.A., 1987. Interactions of diatomic molecules with graphite. Langmuir 3, 1123–1127.
Bonaccurso, E., Kappl, M., Butt, H.-J., 2002. Hydrodynamic force measurements: boundary slip of water on hydrophilic surfaces and electrokinetic effects. Phys. Rev. Lett. 88, 076103.
Chan, D.Y.C., Horn, R.G., 1985. The drainage of thin liquid films between solid surfaces. J. Chem. Phys. 83, 5311–5324.
Churaev, N.V., Sobolev, V.D., Somov, A.N., 1984. Slippage of liquids over lyophobic solid surfaces. J. Coll. Interface Sci. 97, 574–581.
Cieplak, M., Koplik, J., Banavar, J.R., 2001. Boundary conditions at a fluid–solid interface. Phys. Rev. Lett. 86, 803–806.
Dujardin, E., Ebbesen, T.W., Krishnan, A., Treacy, M.M.J., 1998. Wetting of single shell carbon nanotubes. Advanced Mat. 10, 1472–1475.
Fowkes, F.M., Harkins, W.D., 1940. The state of monolayers adsorbed at the interface solid–aqueous solution. J. Am. Chem. Soc. 62, 3377–3386.
Gee, M.L., McGuiggan, P.M., Israelachvili, J.N., Homola, A.M., 1990. Liquid to solid like transitions of molecularly thin films under shear. J. Chem. Phys. 93, 1895–1906.
Gogotsi, Y., Libera, J.A., Güvenç-Yazicioglu, A., Megaridis, C.M., 2001. In situ multiphase fluid experiments in hydrothermal carbon nanotubes. Appl. Phys. Lett. 79, 1021–1023.
Granick, S., 1991. Motion and relaxations of confined liquids. Science 253, 1374–1379.
Helmholtz, H., von Piotrowski, G., 1860. Über reibung tropfbarer flussigkeiten. Sitzungsber. Kaiser. Akad. Wissensch. 40, 607–658.
Israelachvili, J., Gee, M., McGuiggan, P., Homola, A., 1988. Dynamic properties of molecularly thin liquid-films. Abstracts of papers of the American Chemical Society 196, 277.
Kassinos, S.C., Walther, J.H., Kotsalis, E.M., Koumoutsakos, P., in press. Flow of aqueous solutions in carbon nanotubes. In: Lect. Notes Comput. Sci.
Koga, K., Gao, G.T., Tanaka, H., Zeng, X.C., 2002. How does water freeze inside carbon nanotubes? Physica A 314, 462–469.
Koplik, J., Banavar, J.R., 1995. Continuum deductions from molecular hydrodynamics. Ann. Rev. Fluid Mech. 27, 257–292.
Lauga, E., Stone, H.A., 2003. Effective slip in pressure-driven Stokes flow. J. Fluid Mech. 489, 55–77.
Loose, W., Hess, S., 1989. Rheology of dense model fluids via nonequilibrium molecular dynamics: shear thinning and ordering transition. Rheol. Acta 28, 91–101.
Schnell, E., 1956. Slippage of water over nonwettable surfaces. J. Appl. Phys. 27, 1149–1152.
Sokhan, V.P., Nicholson, D., Quirke, N., 2001. Fluid flow in nanopores: an examination of hydrodynamic boundary conditions. J. Chem. Phys. 115, 3878–3887.
Sokhan, V.P., Nicholson, D., Quirke, N., 2002. Fluid flow in nanopores: accurate boundary conditions for carbon nanotubes. J. Chem. Phys. 117, 8531–8539.
Thompson, P.A., Robbins, M.O., 1990. Shear flow near solids: epitaxial order and flow boundary conditions. Phys. Rev. A 41, 6830–6841.
Thompson, P.A., Troian, S.M., 1997. A general boundary condition for liquid flow at solid surfaces. Nature 389, 360–362.
Travis, K.P., Gubbins, K.E., 2000. Poiseuille flow of Lennard–Jones fluids in narrow slit pores. J. Chem. Phys. 112, 1984–1994.
Travis, K.P., Todd, B.D., Evans, D.J., 1997. Departure from Navier–Stokes hydrodynamics in confined liquids. Phys. Rev. E 55, 4288–4295.
van Gunsteren, W.F., Berendsen, H.J.C., 1977. Algorithms for macromolecular dynamics and constraint dynamics. Mol. Phys. 37, 1311–1327.

Vinogradova, O.I., 1999. Slippage of water over hydrophobic surfaces. Int. J. Miner. Process. 56, 31–60.
Walther, J.H., Jaffe, R., Halicioglu, T., Koumoutsakos, P., 2001. Carbon nanotubes in water: structural characteristics and energetics. J. Phys. Chem. B 105, 9980–9987.
Walther, J.H., Jaffe, R.L., Kotsalis, E.M., Werder, T., Halicioglu, T., Koumoutsakos, P., 2004. Hydrophobic hydration of C_{60} and carbon nanotubes in water. Carbon 42, 1185–1194.
Werder, T., Walther, J.H., Jaffe, R., Halicioglu, T., Noca, F., Koumoutsakos, P., 2001. Molecular dynamics simulations of contact angles of water droplets in carbon nanotubes. Nano Lett. 1, 697–702.
Werder, T., Walther, J.H., Jaffe, R.L., Halicioglu, T., Koumoutsakos, P., 2003. On the water–graphite interaction for use in MD simulations of graphite and carbon nanotubes. J. Phys. Chem. B 107, 1345–1352.